Archaeological and Anthropological Sciences (2023) 15:195
https://doi.org/10.1007/s12520-023-01887-1

RESEARCH

Surface treatment techniques of ceramic molds for iron casting from the late Warring States period at the ancient capital city site of Zhu state

Weixin Wang[1] · Guoquan Lu[1] · Song Jiang[1] · Puwen Song[1] · Qing Wang[1]

Received: 27 August 2023 / Accepted: 29 October 2023 / Published online: 28 November 2023

Abstract
A collection of ceramic molds for iron casting from the late Warring States period has been unearthed at the ancient capital city site of Zhu (邾) state in Zoucheng City, Shandong Province. An array of analytical techniques was employed to examine their superficial layers and coatings, including wavelength-dispersive X-ray fluorescence spectrometry, X-ray diffraction, Fourier-transform infrared spectroscopy, scanning electron microscopy with energy-dispersive spectrometry, and polarized light microscopy. The results revealed that the coatings used talc, bone ash (hydroxyapatite), lime plaster (calcite), and analcime as release agents to facilitate the removal of castings from the molds, with analcime being the earliest known used for this purpose. These high-performance, reusable coatings significantly improved the casting efficiency and surface quality of the products. Comprehensive evidence from the compositional, surface, and cross-sectional structural features indicates that the fabrication technique of the surface layer is similar to that of modern immersion coating methods. Using hydrated lime as a binder can efficiently create a smooth surface layer on ceramic molds. Collectively, these technologies supported the iron casting industry in the production of thin-walled, ductile cast iron farm tools with low iron consumption. They embody technological choices and systems that sought to optimize efficiency, quality, and cost-effectiveness.

Keywords Iron casting · Ceramic molds · Surface treatment · Release agents · Analcime · Zhu state

Introduction

The Warring States period marked a pivotal stage in the rapid development of ancient Chinese iron metallurgy and casting. The widespread availability of high-strength, low-cost iron tools significantly liberated productive forces, propelling economic growth, and societal advancement. The highly advanced bronze metallurgy provided a solid foundation for ceramic mold casting technology, elevating it to the most essential craft industry sector. During this period, the majority of iron tools were cast iron (Hua 1999), further underscoring the significance of ceramic mold casting technology.

As an indispensable tool in metal-casting production, the use of ceramic molds for casting metal implements can be traced back to the Erlitou period and spans throughout ancient Chinese history. The pioneering study by Karlbeck (1935) on ceramic molds excavated from the Yin ruins of Anyang laid the groundwork in this field, the first to propose the "piece-mold casting technique." Subsequent research into ceramic molds has largely focused on material composition, surface design, fabrication techniques, physical properties, and casting technology (Freestone et al.1989; Liu et al. 2013; Lukas 2006; Yue et al. 2015; Tan et al. 1999; Liu 2018), providing deeper insights into their production and usage. In recent years, scholars have turned their attention to the organization of ceramic mold artisans' production (Cheng and Chen 2022) and the treatment of mold surfaces (Wang et al.2023). The use of mold coatings has been identified at many different foundry sites across China, including those unearthed at the Yin ruins of Anyang, the Zhouyuan site in Shaanxi's Guanzhong region, the Houma foundry site in Shanxi, the Linzi city site of Qi state, and kiln site in Wen County, Henan, China. Studies have shown that the mirror molds from the Linzi city site of Qi state had surfaces treated with a delicate layer of plant ash and clay to assist

✉ Guoquan Lu
luguoqan@126.com

[1] School of History and Culture, Shandong University, Jinan 250100, China

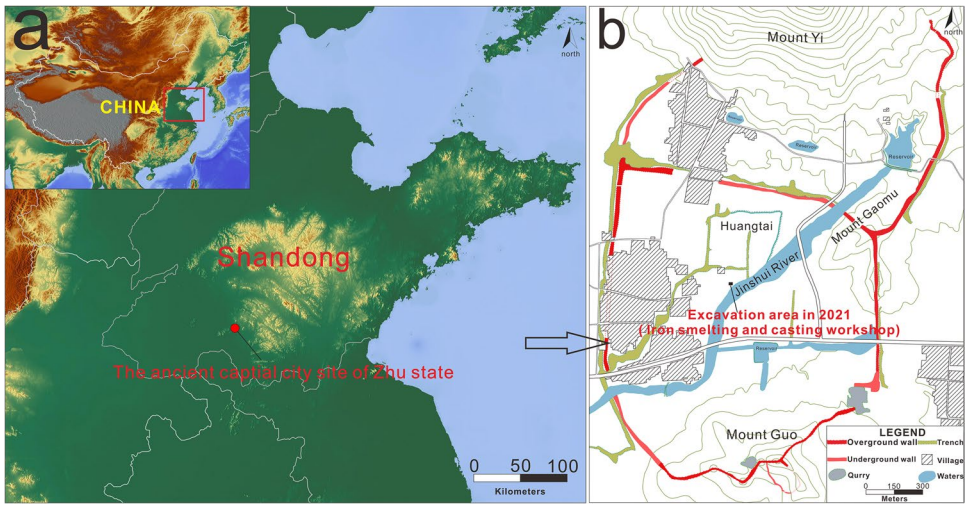

Fig. 1 **a** Location of the ancient capital city site of Zhu state; **b** location of the iron smelting and casting workshop

with demolding (Cui 2020). Ceramic molds from the Houma Baidian foundry site featured surface treatments comprising gypsum, bone ash, and beeswax, which facilitated the release of castings and improved surface smoothness (Wang et al. 2023).

However, most existing research has focused on ceramic molds used for casting bronze-ware. With regard to the iron smelting and casting industry in the Warring States period, researchers (Liu et al. 2022) have paid more attention to the ironware, and there have been relatively few studies of the ceramic molds for iron-casting. Compared to bronze, iron has a higher melting point, imposing different requirements on ceramic mold casting technology and necessitating appropriate surface treatment techniques as the key determinants of successful ironware casting. Examining the surfaces of ceramic molds for iron-casting allows us to understand their materials and fabrication techniques, and to reveal their technological features. To help better understand the iron-casting technology in ancient China, we conducted complementary analyses using various scientific methods on the late Warring States period ceramic molds for iron-casting excavated from the ancient capital city site of Zhu state, to identify their surface material compositions and functions, ascertain surface structural features and production technologies, and analyze the characteristics of their technological systems. It is expected to give deep understanding of the ceramic mold casting technology and manufacturing process of ironware during the Warring States period, and provides new scientific and technical evidences for archaeometallurgy.

Material and methods

Materials

The archaeological materials employed in this study were derived from the ancient capital city site of Zhu state, Zoucheng City, Shandong Province, China (Fig. 1a). Situated at the southern foot of Mount Yi (峄山), the site served as the capital of Zhu state during the mid-Spring and Autumn to Warring States periods (Lu and Wang 2018). Following the demise of Zhu state, it remained the local political, economic, and cultural center. The city features a multitude of functional zones, including palace, storage, pottery workshop, and metallurgical workshop areas. In 2021, the School of History and Culture at Shandong University conducted an excavation of the metallurgical workshop (DMS coordinates: 35°18′29.401″, 117°1′9.858″[1]) located on the northern bank of the Jinshui River (金水河), exposing an iron smelting and casting workshop (Fig. 1b). Numerous ceramic molds (Table S1) and ceramic supports for annealing (Table S2) were unearthed. Judging by their shapes and the surrounding abundance of iron oxide residues, these ceramic molds were used for casting iron farming implements. According to stratigraphic methods and associated pottery morphology, their dating can be traced back to the late Warring States period (BC 312–BC 221).

A total of 18 ceramic mold specimens were selected for this study: 9 shovel (chan), 3 spade (cha), 1 adze (ben), and 5 flat molds. They are all unearthed from a small house site (F2) and two waste pits (H4 and H52) near it and most feature surface coatings; detailed descriptions are provided in Table S1. On the basis of color variations, the ceramic

[1] The coordinates of the workshop, measured using Huace Zhonghui i80 RTK measurement system, in CGCS2000 coordinate system.

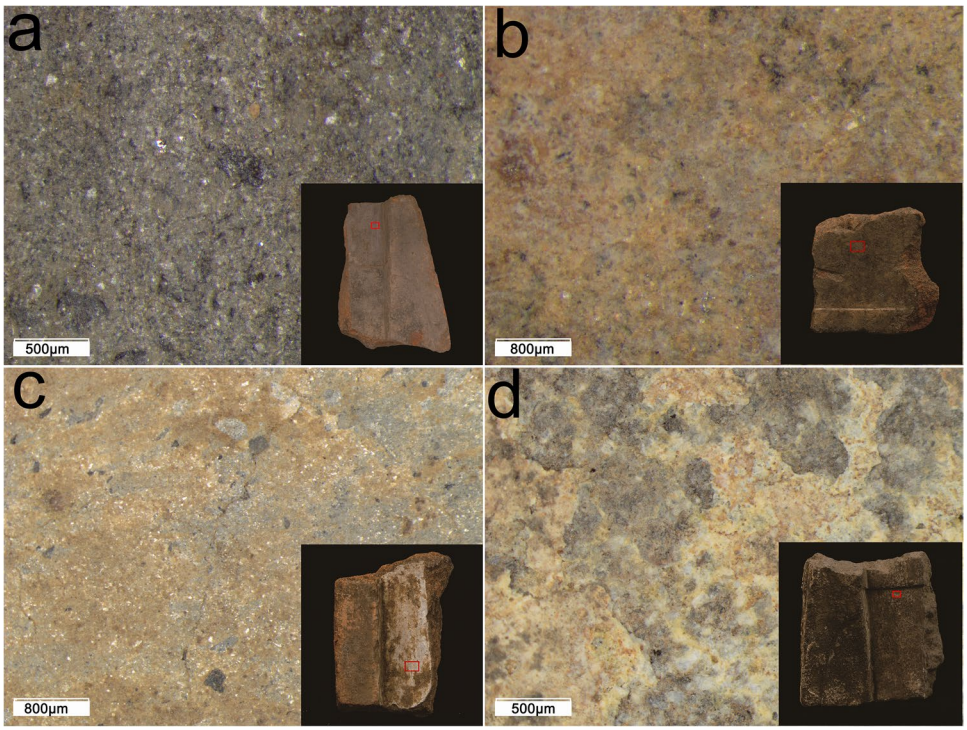

Fig. 2 Microscopic images of the surface of the ceramic molds (**a** silver-gray coating on F2①: 16; **b** brown coating on F2①: 37; **c** white coating and bluish-gray superficial layer on H4: 9; **d** thick grayish-white coating and grayish-black ceramic matrix of F2①: 19)

mold surface coatings can be divided into four categories: (1) silvery-gray coatings ($n=4$) (Fig. 2a); (2) brown coatings ($n=4$) (Fig. 2b); (3) white coatings ($n=2$) (Fig. 2c); and (4) thicker grayish-white coatings ($n=5$) (Fig. 2d), all of which appear crystal-like under microscopic observation. Molds coated with the first three types of coating have red ceramic matrices, whereas the fourth type is applied to grayish-black ceramic matrix containing a substantial amount of sand particles. After the coatings were peeled away, most ceramic molds revealed smooth, bluish-gray superficial layers; however, this structure was not observed in molds treated with the fourth type of coating, which exposed a rough ceramic matrix when the coatings were peeled away (Fig. 2d). In addition, some ceramic molds exhibited a thin, grayish-white layer of deposits on their sides and backs (Fig. 3).

Methods

X-ray fluorescence spectrometer (XRF) was used to detect the chemical composition on the surface of ceramic molds. Coatings, superficial layers, side attachments, and ceramic matrixes were scraped from the ceramic molds with a scalpel, ground into powder samples in an agate mortar and analyzed for chemical composition using a Rigaku ZSX Primus II wavelength-dispersive X-ray fluorescence spectrometer (WDXRF). The elements detected included Si, Al, Fe, Ca, Na, K, Mg, Ti, P, S, Mn, Ba, Co, Zr, and Cl, with results presented in oxide form. The testing conditions were as follows: vacuum, Rh target, tube voltage of 60 kV, current of 50 mA, and a beam diameter of 30 mm.

X-ray diffraction (XRD) was used to characterize the phase compositions of the coatings to identify their categories. The coatings were ground into powders of approximately 80 μm and examined using Rigaku's SmartLab high-resolution X-ray diffractometer. Instrument parameters were as follows: Cu target, vacuum atmosphere, and diffraction angle 2θ from 5° to 65°. Data analysis and phase identification were conducted using Jade 6.5 software.

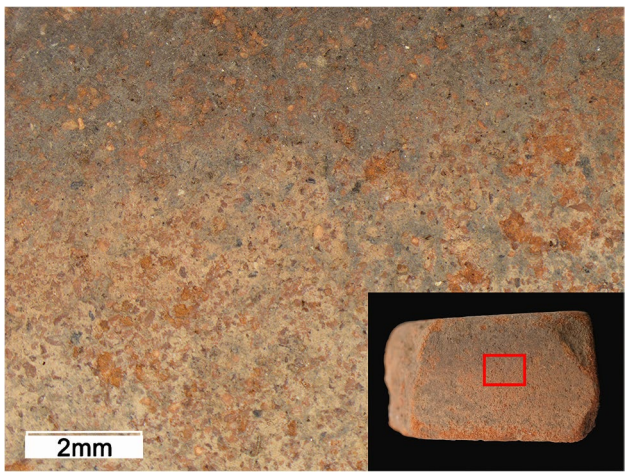

Fig. 3 Grayish-white attachment on the side of the ceramic mold F2①: 42

Fourier-transform infrared spectroscopy (FTIR) was used to further characterize the coating phase. After drying the powdered coating samples to eliminate the interference of free water on the test results, 2 mg of each sample was added to 200 mg of KBr powder (AR, Sinopharm Chemical, China), thoroughly ground, mixed, and pressed into semi-transparent thin slices using a tablet press. Sampling tests were performed using a Bruker ALPHA II Fourier transform infrared spectrometer, with a resolution of 2 cm^{-1} and a detection range of 400–4000 cm^{-1}.

Scanning electron microscope-energy dispersive spectrometer (SEM–EDS) and polarizing microscope were used to observe the surface microstructure of the samples. The cross sections were prepared by precisely sawing the samples, which were then impregnated and embedded in epoxy resin. They were subsequently polished using sandpapers of 600, 1000, and 3000 grit to remove scratches, followed by polishing with 3- and 0.5-μm-diamond suspensions. The gold-coated polished specimens were examined using a Thermo Scientific Quattro S scanning electron microscope (SEM) to observe their microstructures, and the elemental distribution was analyzed using a Bruker X flash 6160 energy dispersive spectrometer (EDS). This aimed to investigate the cross-sectional structure of the ceramic molds and understand the application process of surface layers and coatings. Transparent petrographic thin sections of 30-μm thickness were prepared and observed under an OLYMPUS BX53M polarizing microscope to assist in determining the structural features of the ceramic mold surfaces.

Results and discussion

Analysis of coating composition and function

Identification of coating components

The WDXRF test results are presented in Table 1. The main components of all sample types are SiO_2, Al_2O_3, and Fe_2O_3, indicating that their fundamental composition is clay. The potential phases were inferred on the basis of the characteristic compositions of the coatings. On the basis of the test results, principal component analysis (PCA) was performed to visualize and explore the relationships between the compositions of different sample types (Fig. 4). PCA is a data statistical method that can simplify the complexity in high-dimensional data by transforming the data into fewer dimensions, and PCA plots are often used to find potential clusters. Data with similar features will cluster in PCA plots, which allows us to intuitively see the similarity between different samples (Lever et al. 2017).

In the PCA scatterplot, the various sample types are distinctly divided into groups according to their compositional features. The compositional features of the ceramic matrices exhibit minimal differences, with noticeable scatter point clustering; only a few data points deviate from the main group, demonstrating a high degree of production standardization. The compositional features of distinct colored coatings differ, whereas similarly colored coatings exhibit analogous characteristics. The four silvery-gray coating samples contain relatively high amounts of MgO; given the lustrous surface features of ceramic molds with such coatings applied, it is speculated that these samples include talc. The four brown coating samples comprise larger quantities of P_2O_5 and CaO, possibly associated with materials containing phosphate, such as bone ash. The two white-coating samples are characterized by high concentrations of CaO, which may be related to calcium minerals such as calcite. The five grayish-white coating samples contain substantial amounts of Na_2O, indicating that certain silicate minerals may exist (Table 1). In addition, compared to the ceramic substrates, most of the coatings contain higher levels of S. Research on the black superficial layer of the Linzi mirror molds suggests that this is caused by smoke treatment of the ceramic mold surface before casting, indicating that these ceramic molds may have undergone casting.

The WDXRF test results provided guidance for the targeted qualitative analysis, and on the basis of these results, the various colored coatings were inferred to have different phase compositions. To confirm this, XRD tests were first conducted to determine the specific phase compositions. Figure 5 a shows the XRD pattern of the silvery-gray coating sample on the surface of ceramic mold F2①:1–1, which exhibits diffraction peaks for quartz, microcline, and chlorite commonly found in clay, in addition to strong diffraction peaks at 9.42°, 18.9°, and 28.2° corresponding to talc (PDF#83–1768) crystal planes, indicating that the coating composition consists of clay and talc. Figure 5 b presents the XRD pattern of the brown-coating sample on the surface of ceramic mold F2①:37, with phase identification results revealing hydroxyapatite, quartz, microcline, and albite. The broad peaks at 31.8°, 50.1°, and 59.9° are consistent with the standard pattern of hydroxyapatite (PDF#74–0565), suggesting that the sample was composed of clay and bone ash. Figure 5 c displays the XRD pattern of the white coating on the surface of ceramic mold H4:9, indicating a phase composition of calcite, quartz, microcline, and sodium feldspar. The strong diffraction peaks at 29.3°, 35.9°, 39.3°, and 47.5° correspond to crystal planes of calcite (PDF#72–1652), which, together with clay, form the raw materials of the white coating. Figure 5 d shows the XRD pattern of the thick grayish-white coating on the surface of ceramic mold F2①:19, with a phase composition consisting of analcime, quartz, microcline, kalsilite, and actinolite. The strong diffraction peaks at 15.8°, 26.0°, and 28.3° are attributed to analcime (PDF#19–1180). Multiple diffraction peaks are consistent

Table 1 WDXRF detection results and composition inference of samples (wt%)

Mold no	Area of analysis	SiO_2	Al_2O_3	Fe_2O_3	CaO	Na_2O	K_2O	MgO	TiO_2	P_2O_5	SO_3	MnO	BaO	Co_3O_4	ZrO_2	Cl	Possible materials
F2①:37	Ceramic matrix	66.152	15.508	9.237	1.726	0.35	3.011	2.50	0.712	0.093	—	0.081	0.278	—	0.051	0.301	—
	Coating	29.609	6.476	2.392	36.111	0.21	1.217	0.796	0.366	21.544	0.870	0.055	0.06	0.007	0.03	0.266	Bone ash
F2③:1	Ceramic matrix	69.475	14.314	6.535	1.570	0.464	3.821	2.547	0.582	0.106	—	0.086	0.155	—	0.061	0.283	—
	Coating	66.728	12.024	5.328	1.411	0.33	2.189	9.238	0.446	0.729	1.023	0.094	0.047	—	0.09	0.323	Talc
F2①:38	Ceramic matrix	63.993	17.827	7.983	1.654	0.719	3.396	2.589	0.719	0.087	—	0.453	0.146	—	0.067	0.370	—
	Superficial layer	59.107	18.707	9.470	5.252	0.526	1.992	2.839	0.759	0.828	—	0.075	0.143	—	0.012	0.290	—
H52:21	Ceramic matrix	70.771	13.181	7.621	1.726	0.459	3.103	1.696	0.668	0.093	—	0.129	0.144	—	0.009	0.400	—
	Superficial layer	63.097	17.035	8.564	4.342	0.498	2.117	2.468	0.761	0.381	0.066	0.056	0.216	—	0.043	0.357	—
F2①:41	Ceramic matrix	66.765	16.075	7.765	1.695	0.497	3.751	2.104	0.575	0.000	—	0.114	0.206	—	0.081	0.372	—
	Coating	63.521	12.050	5.888	2.103	0.808	3.397	8.754	0.703	0.626	1.532	0.086	0.132	0.002	0.031	0.366	Talc
F2①:22	Ceramic matrix	64.411	16.286	10.014	2.501	0.318	2.749	2.283	0.635	0.127	0.000	0.120	0.220	—	0.021	0.315	—
	Coating	55.163	15.615	8.16	3.536	8.612	2.115	1.628	0.87	3.218	0.235	0.216	—	0.03	0.044	0.558	Unknown silicate
	Side attachment	57.161	16.137	6.557	3.032	8.776	1.928	1.565	0.799	2.854	0.336	0.193	0.002	0.031	0.056	0.573	Unknown silicate
F2③:3	Ceramic matrix	69.080	14.195	6.852	1.731	0.368	2.656	2.626	0.627	0.152	1.116	0.084	0.116	—	0.066	0.332	—
	Coating	66.283	13.399	9.164	3.846	0.971	2.358	4.795	0.662	1.127	5.426	0.035	0.052	—	0.031	0.294	Talc
	Superficial layer	59.540	16.554	8.913	5.966	1.013	1.927	3.232	0.391	0.815	0.079	0.158	0.098	—	0.033	0.376	—
	Side attachment	60.472	16.192	9.017	5.795	0.997	2.086	2.378	0.429	0.561	0.047	0.133	0.104	0.012	0.048	0.312	—
F2①:42	Ceramic matrix	66.198	16.801	8.381	1.844	0.726	2.331	1.883	0.570	0.058	0.423	0.109	0.188	—	0.075	0.413	—
	Coating	45.871	9.379	5.328	11.712	0.930	2.137	2.080	0.645	14.523	2.975	0.144	0.164	0.007	0.069	0.387	Bone ash
	Superficial layer	62.054	15.172	9.428	6.041	0.723	1.779	1.721	0.556	1.208	0.668	0.097	0.123	—	0.084	0.346	—
	Side attachment	60.708	14.919	10.257	6.167	1.257	2.320	1.427	0.714	1.414	0.096	0.091	0.146	0.006	0.087	0.394	—
F2①:16	Ceramic matrix	68.092	14.530	7.676	1.673	0.648	3.279	2.297	0.707	0.491	0.022	0.080	0.161	0.000	0.071	0.274	—
	Coating	65.752	7.778	5.969	1.302		2.189	13.796	0.348	0.486	1.859	0.114	0.042	0.027	0.04	0.298	Talc
	Superficial layer	58.691	14.858	9.88	7.875	1.024	2.363	3.462	0.624	1.406	0.119	0.075	0.146	—	0.038	0.439	—
H4:5	Ceramic matrix	64.737	17.240	8.734	1.953	0.406	3.281	2.171	0.634	0.076	—	0.184	0.256	—	0.000	0.325	—
	Coating	42.579	11.566	17.694	15.913	0.544	1.084	4.089	0.465	5.635	—	0.120	0.092	—	0.042	0.177	Bone ash
F2①:36	Ceramic matrix	66.818	16.440	8.086	1.920	0.317	3.256	1.910	0.633	0.056	—	0.084	0.156	0.019	0.066	0.237	—
	Coating	41.750	8.276	5.725	36.637	0.663	2.544	1.142	0.693	0.713	1.436	0.035	0.093	0.009	0.054	0.227	Calcite
H378:8	Ceramic matrix	71.709	12.945	7.022	1.770	0.564	2.873	2.253	0.324	0.024	—	0.075	0.190	—	0.017	0.333	—
	Superficial layer	61.024	14.224	8.528	8.839	0.490	1.315	3.078	0.768	0.896	0.023	0.085	0.171	—	0.057	0.504	—
H4①:36	Ceramic matrix	65.580	17.496	7.983	1.671	0.746	2.465	2.127	1.143	0.164	—	0.098	0.131	—	0.034	0.362	—
	Coating	43.610	10.564	6.937	20.838	0.303	2.756	0.747	0.444	13.344	—	0.053	0.069	0.012	0.038	0.286	Bone ash
H4:9	Ceramic matrix	66.275	17.671	7.649	1.685	0.558	2.603	2.134	0.628	0.000	—	0.089	0.187	—	0.086	0.435	—
	Coating	36.917	7.324	3.493	48.036	0.361	1.744	1.35	0.398	0.066	—	0.094	0.064	0.011	0.031	0.111	Calcite
F2①:19	Ceramic matrix	63.766	16.436	9.875	2.540	0.415	3.717	1.773	0.638	0.089	—	0.129	0.212	0.008	0.006	0.396	—
	Coating	54.628	17.941	5.558	3.832	10.716	2.326	1.265	0.799	1.854	0.336	0.193	0.002	0.031	0.056	0.463	Unknown silicate

Table 1 (continued)

Mold no	Area of analysis	SiO_2	Al_2O_3	Fe_2O_3	CaO	Na_2O	K_2O	MgO	TiO_2	P_2O_5	SO_3	MnO	BaO	Co_3O_4	ZrO_2	Cl	Possible materials
F2①:1–1	Ceramic matrix	64.330	16.022	10.079	2.629	0.447	2.802	1.604	0.893	0.138	0.035	0.247	0.175	—	0.056	0.545	—
	Coating	57.803	17.253	8.547	2.876	7.379	1.957	2.077	0.529	0.033	0.969	0.086	0.146	—	0.063	0.283	Unknown silicate
F2①:1–2	Ceramic matrix	59.411	18.959	12.578	2.664	2.664	1.174	1.623	0.735	0.123	—	0.305	0.160	—	0.016	0.588	—
	Coating	56.176	18.470	7.787	3.571	7.988	2.042	1.469	0.634	0.144	0.839	0.176	0.204	—	0.022	0.478	Unknown silicate
F2①:1–3	Ceramic matrix	61.441	17.891	11.896	2.163	1.299	1.088	1.883	0.947	0.297	0.048	0.238	0.390	0.005	0.037	0.376	—
	Coating	58.680	17.154	8.084	1.943	8.668	1.450	2.336	0.564	0.174	0.130	0.089	0.327	—	0.044	0.358	Unknown silicate

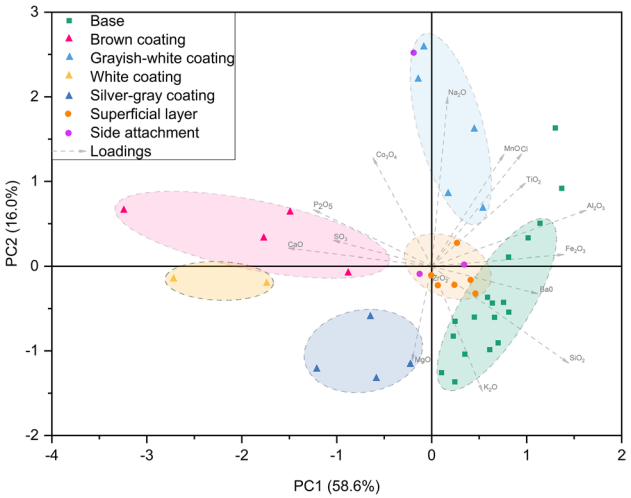

Fig. 4 PCA results of sample WDXRF data

with the standard diffraction patterns of analcime but differ significantly from the standard diffraction patterns of other silicate minerals. The FOM value that reflects the degree of matching reached 1.3, reflecting a high matching degree with analcime. Analcime is a silicate mineral with a high Na content, which together with clay forms the raw materials of the grayish-white coating. The site is situated near the Mount Yi; Neoarchean magmatic rocks are widely exposed within the site, mainly in the Yishan sequence, consisting of intermediate-acidic diorite and granite (Wang et al. 2012). Natural analcime can form under magmatic and hydrothermal conditions (Ghobarkar and Schäf 1999). Therefore, the geological conditions at the site allow for the production of analcime. It is possible that craftsmen discovered this mineral and employed it in the fabrication of ceramic molds. The XRD test results were generally consistent with the inferences made on the basis of the WDXRF test results.

FTIR analysis was then conducted to characterize the phase composition of the coatings and further verify the accuracy of the XRD test results. FTIR analysis of the silvery-gray coating and ceramic matrix of ceramic mold F2①:16 revealed that the coating material spectra matched well with talc spectra (Fig. 6a), with the absorption peak at 3678 cm^{-1} corresponding to the bending vibration absorption peak of Mg–OH; the broad peak at 3469 cm^{-1} corresponding to the stretching vibration of –OH; the absorption peak at 1635 cm^{-1} corresponding to the bending vibration absorption peak of interlayer water in talc; the strong peak at 1016 cm^{-1} attributed to the asymmetric stretching vibration of Si–O; and the absorption peaks near 670 and 451 cm^{-1} caused by the bending vibration of Si–O–Mg, with the absorption peak at 529 cm^{-1} corresponding to the stretching vibration absorption peak of O–Mg (Zhang et al. 2006). The infrared spectrum of the

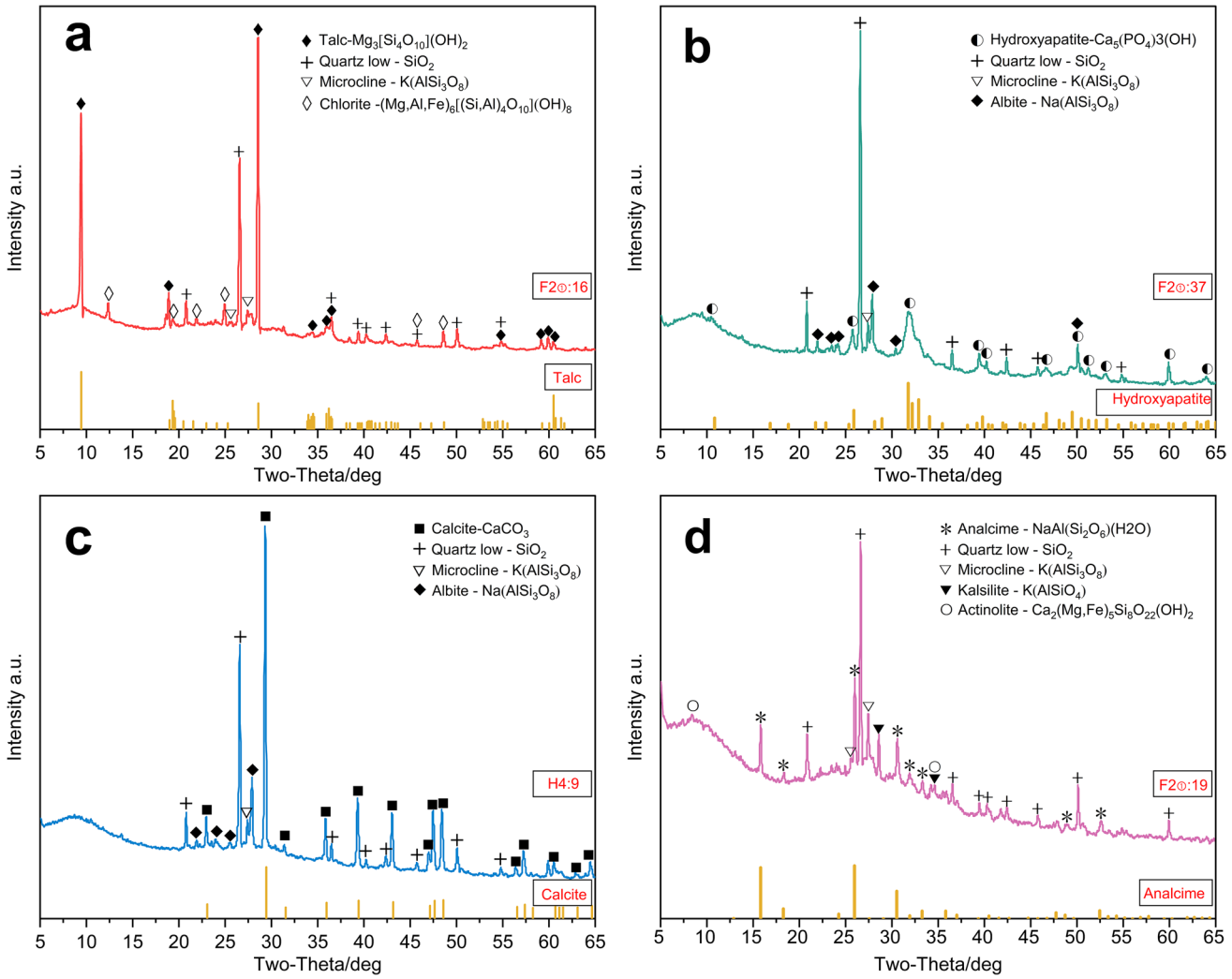

Fig. 5 XRD analysis results of surface coatings on the samples (**a** silver-gray coating on F2①:16; **b** brown coating on F2①:37; **c** white coating on H4:9; **d** grayish-white coating on F2①:19. The orange bar charts represent the standard XRD spectrum of special materials added to the coating)

brown coating on the surface of ceramic mold F2①:37, when compared to the ceramic matrix exhibits several additional absorption peaks, with the peak at 3585 cm^{-1} corresponding to the stretching vibration of hydroxyl (–OH) in the structural water, the peak at 1039 cm^{-1} corresponding to the asymmetric stretching vibration peak of the PO_4^{3-} group, and the absorption peaks at 604 and 568 cm^{-1} attributed to the bending vibration of the PO_4^{3-} group (Cui et al. 2017). These absorption peaks correspond well with hydroxyapatite characteristic peaks in bone ash, indicating that bone ash was added to the coating. The characteristic peaks of CO_3^{2-} appear at 1418 and 1453 cm^{-1}, which may be related to the partial replacement of PO_4^{3-} by CO_3^{2-} during the burial process (Fig. 6b). Figure 6 c shows the infrared spectra of the white coating and ceramic matrix of the ceramic mold H4:9 and of calcite. Compared to the ceramic matrix, the coating spectrum features several additional absorption peaks, with the peak at 1797 cm^{-1} representing C–O stretching vibration and, those at 1457 cm^{-1}, 873 cm^{-1}, and 713 cm^{-1} corresponding, respectively, to the asymmetric stretching vibration, the out-of-plane bending vibration and the in-plane bending vibration of CO_3^{2-} (Weng and Xu 2016), exhibiting a good match with the standard infrared spectrum of calcite. Considering the characteristics of the v_3 (1457 cm^{-1}), v_2 (873 cm^{-1}), and v_4 (713 cm^{-1}) peaks (Vikki et al. 2008), and the loose powdery texture of the coating, these calcites should be artificially applied plaster, converted from hydrated lime. FTIR testing of the grayish-white coating and ceramic substrate of ceramic mold F2①:19 (Fig. 6d) revealed a good match between the grayish-white coating and analcime, with three absorption peaks at 3614 cm^{-1}, 3432 cm^{-1}, and 1621 cm^{-1} representing characteristic peaks of zeolite water, corresponding,

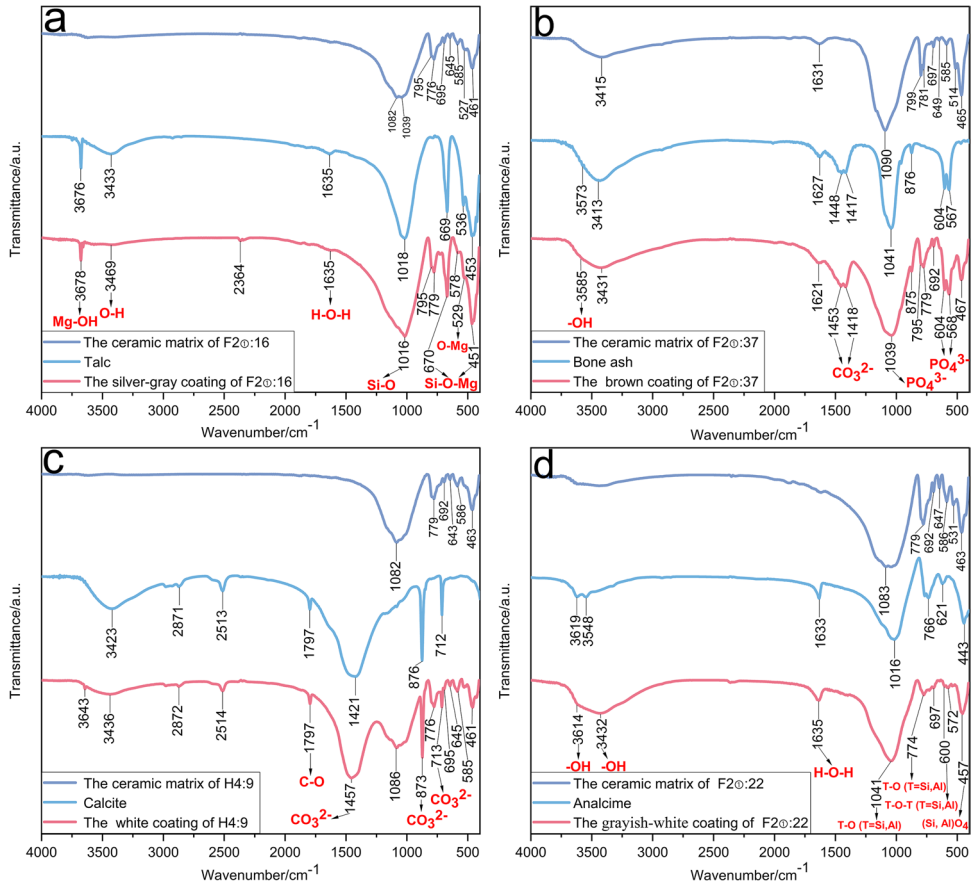

Fig. 6 Infrared spectrum of coatings and ceramic matrixes of the samples (**a** silver-gray coating on F2①:16; **b** brown coating on F2①:37; **c** white coating on H4:9; **d** grayish-white coating on F2①:19)

respectively, to the stretching vibration of hydrogen bonds (O–H) in zeolite water, the stretching vibration of hydroxyl (–OH), and the bending vibration of O–H–O. The infrared spectrum in the region of 1300–200 cm^{-1} is a fingerprint of the region indicating structural features of zeolite frameworks (Flanigen et al. 1974). The absorption peaks at 1041 cm^{-1} and 774 cm^{-1} correspond to the asymmetric stretching vibrations of T–O (T = Si, Al), with the peak at 600 cm^{-1} related to the internal bending vibrations of T–O–T (T = Si, Al), and the spectral band at 457 cm^{-1} caused by the internal vibrations of [(Si, Al) O_4] tetrahedra in analcime (Azizi and Yousefpour 2010). The above characteristic peaks are consistent with analcime. These results validate the effectiveness of the XRD analysis.

Function of coating materials

Currently, scholars (Li 1991; Dong et al. 2011) often attribute the coatings on the surface of the ceramic molds for iron casting to the residual traces left after the casting process, while WDXRF, XRD, and FTIR scientific analysis methods determined the composition of the coatings on the surface of the ceramic molds for iron casting from the ancient capital city site of Zhu state, providing a basis for further exploration of their specific functions.

The silvery-gray coating contained talc. In modern casting processes, talc is often used as a refractory aggregate for casting coatings. Its melting point reaches 1550 °C, offering excellent fire resistance, and its layered structure provides good lubrication and water repellency, facilitating demolding (Nwaogu and Tiedje 2011). From the Eastern Zhou to the Qin and Han periods, China used talc molds extensively for coin casting (Huang 2017). Talc molds for casting coins from the Western Han period have been discovered in Zoucheng City too (Cheng 2000), where the ancient capital city site of Zhu state is located. The use of talc powder coatings can be seen in ceramic molds unearthed in Wen County (Hua 1999). Talc might be added to facilitate the demolding of castings and prevent the adherence of molten iron to the ceramic mold body, which would have damaged the mold.

The brown coating contained bone ash (hydroxyapatite), which has a melting point of 1650 °C and is an excellent refractory material (Yu 2021). Chastain (2019) claimed that bone ash was detected on the surface of ceramic molds from the Houma foundry, Zhougongmiao site, and the ancient capital city site of Zheng and Han state, while Wang et al. (2023) pointed out that applying bone ash to the surface of ceramic molds is related to easier demolding of castings and improving their surface quality, and that this material was prevalent at the Houma Baidian foundry site.

The white coating contained lime plaster (calcite). The use of lime plaster as a type of coating has a long history and has been widely used in ancient architecture and other artifacts for surface decoration or protection (Kingery et al. 1988; Adi et al. 2016). Its excellent permeability and leveling property can form a solid and flat coating layer on the rough ceramic matrix. Application of lime plaster to the surface of ceramic molds can be seen in the ceramic molds from the Zhouyuan site (Chastain 2019) and those for iron casting from the Linzi city site of Qi state (Li 2020). Calcite will produce calcium oxide and CO_2 gas under high-temperature conditions; calcium oxide has a melting point of 2600 ℃, making it an excellent refractory material (Routschka 1997). However, materials with large gas evolution are harmful to the casting. The air gap between castings and molds is usually regarded as one of the reasons for surface defects (gas cavities, cracks, etc.) of castings (John 2015). But ceramic molds were usually preheated before casting to prevent bursting (Yang 2004). After this process, the defect of gas release from the coating may have been effectively avoided. To summarize, the lime plaster on the surface of the ceramic molds can separate the molten iron and the ceramic matrix, which could play an important role in preventing molten iron from permeating into the porous ceramic matrix and reacting with the ceramic matrix of fusible clay texture to form sand burning. Therefore, the calcite may have served as a release agent on the surface of the ceramic mold and protected the fusible ceramic matrix.

The grayish-white coating contained analcime. The addition of analcime coating also prevented the direct contact between molten iron and the fusible ceramic matrix, thus preventing the occurrence of sand burning and allowing the castings to be demolded without harming the ceramic molds. Meanwhile, as a kind of zeolite mineral, analcime has good absorbability due to its internal pores and large specific surface area. It can strongly adsorb gases such as H_2O and CO_2 (Long et al. 2016), which may have been produced during the casting process. This property probably helped reduce the air gap between the castings and the ceramic molds and improve the surface quality of the castings. Moreover, the ability of zeolite to absorb polar molecules like H_2O and CO_2 is reversible (Rute et al. 2019). By preheating before casting to remove absorbed gas impurities in the internal pores of analcime, this ability can be repeatedly and continually obtained. In addition, analcime also has a high porosity rate (Cataldo et al. 2021), which can improve the permeability of the ceramic molds and enhance the filling capacity of the molten metal, thus improving the quality of castings. Approximately 2700 years ago, the ancient Romans and Greeks used building materials containing zeolite when constructing hydraulic structures (Jackson et al. 2017). Moreover, the ancient Mayans built the oldest known zeolite water purification filtration system in Corriental reservoir at Tikal, an ancient Maya city in Guatemala in ~ 2185 cal year BP. They used clinoptilolite as a water purifier, which has excellent adsorption properties to absorb harmful substances in water (Tankersley et al. 2020). The age of ceramic molds from the ancient capital city site of Zhu state dates to the late Warring States Period (BC 312–BC 221), representing the most ancient case of analcime usage currently known and the earliest known application of the reversible adsorption of zeolite minerals. At that time, people may have discovered certain special properties of zeolite minerals and used analcime as a reusable release agent.

In summary, the talc, bone ash (hydroxyapatite), lime plaster (calcite), and analcime materials on the surface of ceramic molds for iron casting from the ancient capital city site of Zhu state may function as release agents to facilitate the demolding of castings and improve the casting surface quality.

Surface structure and manufacturing process analysis

Structural analysis results

SEM analysis was conducted on the cross sections of the ceramic molds. The results show that the cross-sectional structures near the surfaces of these molds can be classified into four types. The first type ($n = 8$), represented by F2①:42 (Fig. 7a), is characterized by a three-layer structure: (1) a thin coating, (2) a superficial layer, and (3) a ceramic matrix with a relatively high concentration of coarse sand. This type of cross-sectional structure is more evident under polarized light microscopy (Fig. 8). The second type ($n = 5$), exemplified by F2①:19 (Fig. 7b), can be divided into two layers: (1) a thicker coating and (2) a ceramic matrix comprising coarse sand and fine clay. Most of the ceramic molds possess these two structural types. The third and fourth types are special variations of the first. The third type ($n = 2$), represented by H4:5 (Fig. 7c), has two coating layers. The bright white areas indicate the presence of metals. This structure indicates the repeated usage for high-intensity casting production activities. Further EDS elemental distribution analysis (Fig. 9) revealed different compositions of the two coating layers, containing higher amounts of Mg and P, respectively,

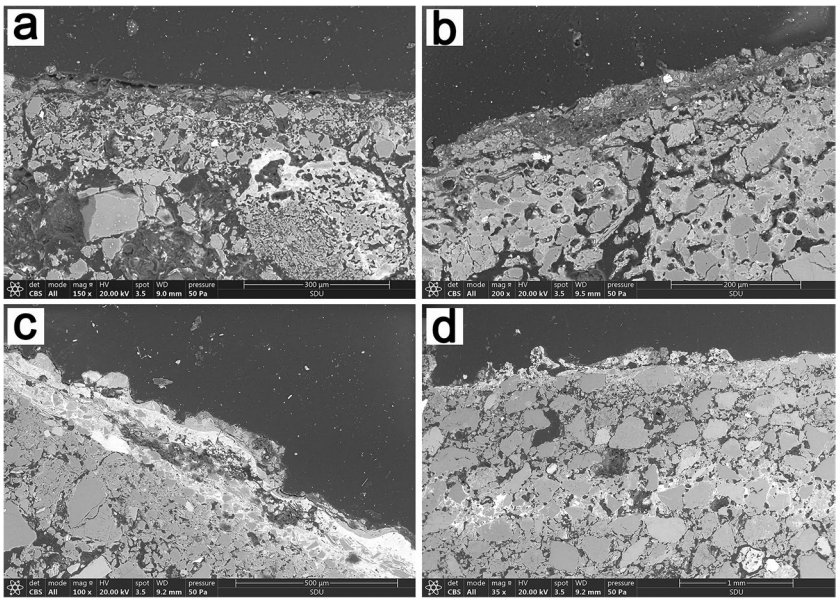

Fig. 7 SEM images of the cross-sectional structure of the ceramic molds (**a** F2①:42; **b** F2①:19; **c** H4:5; **d** H378:8)

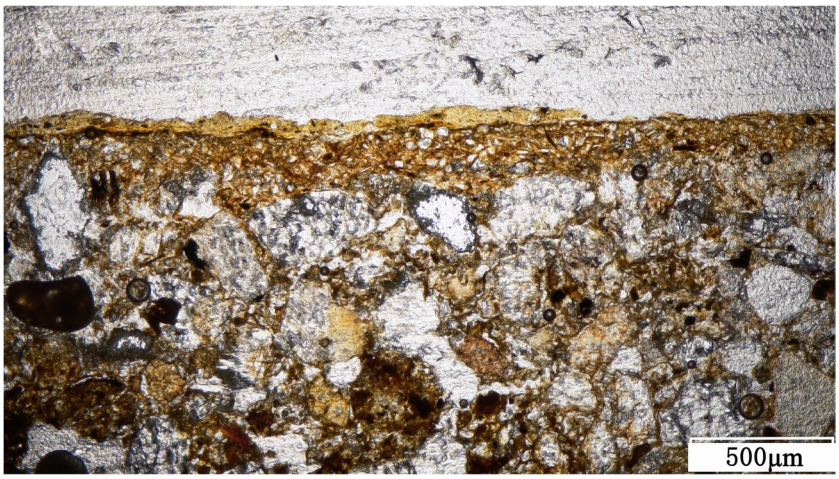

Fig. 8 Microstructure of ceramic mold F2①: 42, under unipolar light

possibly indicating the sequential use of talc and bone ash for demolding purposes. The fourth type ($n=3$), exemplified by H378:8 (Fig. 7d), exhibits a ceramic matrix containing a substantial amount of coarse sand and an extremely thin surface layer, with the coating layer almost entirely detached. A common feature among these four types is the relatively smooth surface or coating layer, with thicknesses ranging from 100 to 200 μm for types one to three. Thin and smooth surface layers are advantageous in reducing surface defects such as sand holes on castings but require a higher level of technical expertise or specialized manufacturing techniques from artisans working on rough ceramic matrix.

Surface manufacturing process

With regard to the manufacturing process of the ceramic mold surface, Liu (2019) inferred that the coatings were brush-applied onto the ceramic matrix, given the presence of brush marks on the surface of the Yin ruins ceramic molds. Wang et al (2023) confirmed this by SEM. However, SEM observations revealed that both the surface and coating layers of the ceramic molds from the ancient capital city site of Zhu state were quite smooth, with no visible brush marks. Evidence from both the surface and composition features of the ceramic molds provides new insights to address this issue. Some ceramic molds have a thin, grayish-white layer of attachment on their sides and backs. The parts near the parting surface were darkened owing to the high temperature (Fig. 3), indicating that they already existed during casting. The PCA grouping results of the chemical compositions showed that their composition was similar to that of the superficial layer (Fig. 4), containing a higher amount of CaO, which is possibly related to the use of hydrated lime as a binder. Hydrated lime was also used as a binder for

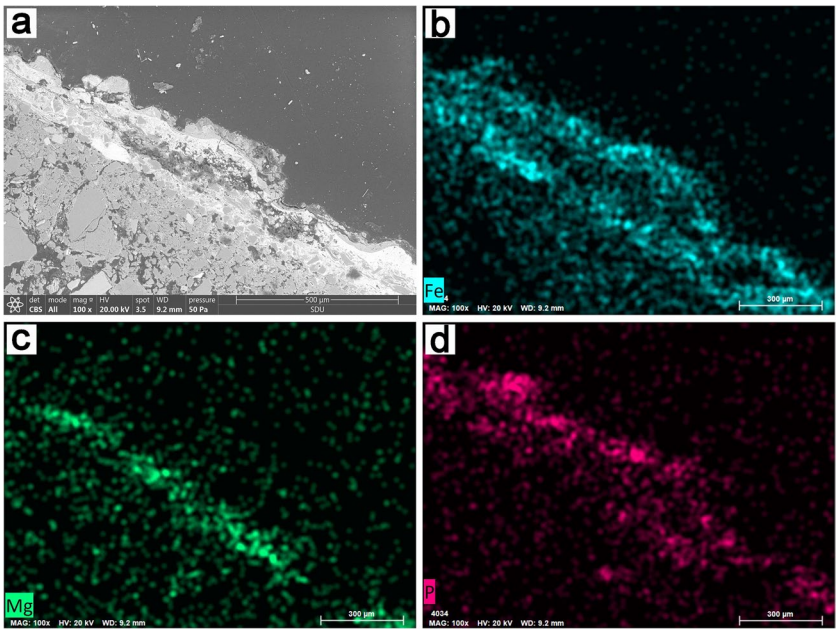

Fig. 9 Mapping of elemental distribution in H4:5 (**a** SEM image, 100×; **b**–**d** the distributions of Fe, Mg, and P)

the ceramic mold bodies in the Yin ruins (Yue et al 2015). Hydrated lime can firmly attach a superficial layer to the ceramic matrix, thereby extending its service life. Thus, the application method of the ceramic mold surface layer might be similar to modern "dip coating" techniques (Gooch 2011). Specifically, clay and hydrated lime are mixed to form a paste, and then the ceramic mold body is dipped into the slurry. After removal, a thin and smooth superficial layer forms on the body, leaving residues on the sides and back. Subsequently, a coating layer is applied on the superficial layer. The above inference is also supported by simulation experiments (see supplementary material-3 for further details). Similar procedures were applied to the ceramic molds with thicker grayish-white coating layers, with the chemical composition of the attachments on the sides and backs is similar to the coating (Fig. 4), indicating that the dip coating method was also employed. However, only one coating layer is present in the ceramic matrix. Considering the unique mechanism of analcime, artisans may intentionally apply a thick and smooth coating layer to replace the superficial layer, thus serving the dual purposes of smoothing the casting surface and facilitating demolding.

Compared with brush painting techniques, dipping methods are simple and efficient, and enhance the quality of the surface layer.

Technological choices and technical system

By analyzing the superficial treatment techniques of the ceramic molds from the ancient capital city site of Zhu state, as well as their ironware production techniques, and comparing them with ceramic molds from other sites, we can summarize the characteristics of the technological choices made in the iron smelting and casting industry of the ancient capital city of Zhu state.

The discovery of a large number of the ceramic supports for annealing (Table S2) reveals that the iron production route at the ancient capital city site of Zhu state involved cast iron-softening technology (Hua 1982). First, the metal was cast into white cast iron (Table S3) and then decarburized through annealing, which reduced the hardness and brittleness while increasing the toughness, resulting in a superior ductile cast iron. To accommodate the annealing process and ensure the successful casting of white cast iron, as well as facilitating its conversion to ductile cast iron, the mold cavity of the ceramic mold is narrow (Fig. 10), casing the thickness of the products to be only approximately 1–2 mm. This thin-walled structure reduced the amount of iron consumed per unit product, increased the cooling rate of the castings, generated more white cast iron structures, and allowed for more thorough annealing, resulting in high-quality ductile cast iron (Hua 1982). The smooth superficial layer improved the evenness of the mold surface, while the coating facilitated mold release; together, these factors enhanced the surface quality of the castings and eliminated the need for potentially damaging polishing processes. This approach embodies the pursuit of quality at the lowest possible cost.

However, the lightweight and thin structure also made the castings prone to wear. Given the widespread demand for iron agricultural implements due to agricultural production, iron implements became consumable products that needed continuous production to meet demand. Under such circumstances, the reusability of pottery molds is important. In fact, multi-layered coating layers (Fig. 8c) have already

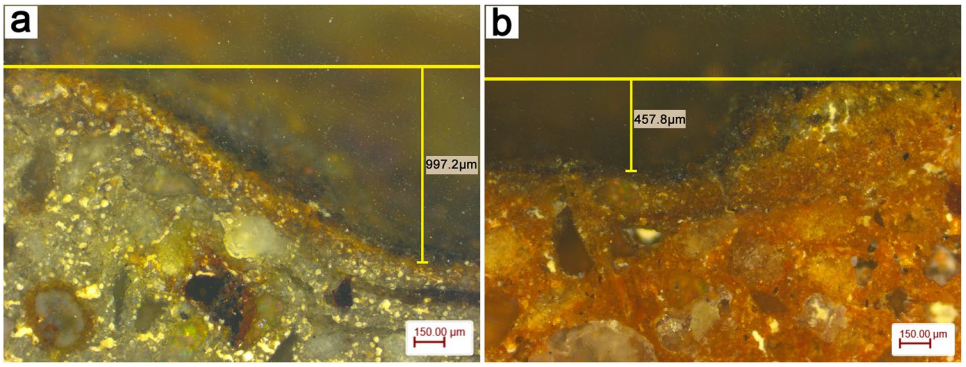

Fig.10 Cross section structure of ceramic molds (**a** shovel (chan) mold F2①: 19; **b** spade (cha) mold F2①: 37)

demonstrated that the ceramic molds at the ancient capital city Site of Zhu state were reused. Moreover, the coating layers provided excellent protection for the fragile ceramic molds. Figures 8 c and 9 show that the molten iron only caused damage to the lower surface coating layer and did not damage the internal ceramic matrix. Above the lower coating, a new layer was coated, suggesting that the coating on the lower surface could have served as a sacrificial surface layer that could be replaced when damaged (for reuse of the mold). Therefore, the existence of the coating layers made it easier to repair the ceramic molds, greatly prolonging their lifespan and further reducing production costs. As the ceramic molds had to be used repeatedly and the surface of the ceramic molds had to withstand multiple impacts from high-temperature molten iron; high demands were placed on the thermal stability and reusability of the surface-coating materials. The inorganic materials used for the surface coatings of ceramic molds for iron casting in the ancient capital city site of Zhu state, such as talc, hydroxyapatite, calcite, and analcime, mostly possess these properties. Compared with the easily thermally decomposable organic materials such as beeswax and grease on the surface of the early Warring States period Houma ceramic molds for bronze casting (Wang et al. 2023), the use of durable inorganic materials is obviously a more advanced, efficient, and cost-effective technological choice.

It is worth noting that there were numerous types of coatings used. As the ceramic molds currently found in the workshop are all gathered in a small house site and two waste pits near it, which suggests that these molds might have been used by the same group of craftsmen within the same period, thus the use of numerous types of coatings might not be due to diachronic changes or the existence of different production groups. Meanwhile, the same type of ceramic mold used different kinds of coatings (Table 1), indicating that each type of coating might all be adaptable to the production of different types of ironware, so there is no sufficient evidence to suggest that different coating materials were chosen to adapt to the production of different ironware.

Considering the natural resource conditions and historical background of the site, the large number of coating types may be related to the resource distribution around the site and the exploration of demolding technology. The mineral resources around the ancient capital city site of Zhu state were scarce(Liu and Miao 1995) and Zhu was a weak state with a small territory, faced with blockades from neighboring enemy states such as Lu (鲁). It would have been difficult for it to obtain high-quality refractory materials from other regions. This may be one of the reasons for the application of other unconventional materials in addition to traditional refractory materials such as talc. Through SEM–EDS analysis of the two coatings on the surface of mold H4:9, it was found that the two coatings contained high levels of Mg and P elements, respectively, indicating that talc and bone ash were used successively in the two stages of the production process. Easily obtained bone ash may have served as an alternative to the scarce talc. Due to limited resources, various more accessible materials have also been used to supplement the shortage of high-quality demolding materials. Meanwhile, this phenomenon might be related to the exploration of demolding technology. Given that the resources were limited, various materials were possibly tested to determine the appropriate coating, causing a series of materials with similar properties that could be substitutes were all used as raw materials of coatings, which allowed for the arbitrary use of a variety of coatings to a certain extent. However, there was still a preference for certain materials. On the surface of the ceramic molds unearthed from the ancient capital city site of Zhu state, materials with high stability and reusability such as talc ($n=4$), bone ash ($n=4$), and analcime ($n=5$), featured in high proportion (13/18) and were widely used, whereas materials such as calcite ($n=2$) with high gas production and slow conversion rate, featured in a lower proportion (2/18). This may reflect a technological preference for high performance and low cost at that time. The large-scale demand for cast iron production prompted people to search for release agents offering the best comprehensive benefits. The use of talc may have been the precursor to the large-scale use of talc molds for casting

during the later Qin and Han dynasties. Use of analcime for mold release was one of the earliest examples of this type of material being employed in metallurgical activities, demonstrating the advanced nature of the technology. It is worth noting that ceramic molds using analcime have a gray-black ceramic matrix, which is significantly different from the red ceramic matrix of other molds, and their superficial layer structure also varies. This may reflect differences in the techniques mastered by the artisans who created these two types of ceramic molds or in the artisan's origins.

In general, to accommodate the large-scale production of ironware, the ancient capital city site of Zhu state developed an iron production technical system during the late Warring States period that pursued efficiency, quality, and low costs, and embodied advanced technological choices. This is particularly evident in the selection of surface treatment technologies for ceramic molds. The use of high-performance coatings and smooth surfaces, along with efficient processing techniques improved the quality and production efficiency of ironware. Reusable ceramic mold coatings and the reduced iron consumption of thin-walled ironware lowered production costs, creating a balance between quality, efficiency, and cost. This allowed the common people to acquire high-quality iron agricultural implements at low prices. This had a positive impact on promoting the popularization of iron implements and reflected the complex interaction and internal consistency in the development of the iron smelting and casting technology system of the ancient capital city site of Zhu state and its socio-economic system.

Conclusion

This study conducted a detailed analysis of the surface portions of the late Warring States period ceramic molds for iron casting unearthed at the ancient capital city site of Zhu state, revealing the material composition and function of the coatings, the application techniques of the superficial layer, and the associated technological choices and technical systems. For iron casting, inorganic materials with excellent performance and reusability such as talc, bone ash (hydroxyapatite), lime plaster (calcite), and analcime, were used as raw materials for ceramic mold coatings to facilitate the release of castings. Notably, analcime was discovered for the first time in a ceramic mold coating material and represents the earliest known case of utilization of the zeolite minerals to aid in the demolding of castings. The superficial layer was fabricated using a simple and efficient dipping process. High-performance coatings and smooth surface layers jointly facilitated the production of thin-walled ironware, forming efficient, low-cost, and quality-focused iron smelting and casting technology system, reflecting the advanced nature of the technological choices. In addition, the ceramic matrix color and surface structure of the ceramic molds with analcime coatings differed from those of other molds. The reasons for this difference warrant further exploration in relation to cultural background and coating performance characteristics. In light of these findings, our understanding of ancient Chinese ceramic mold-casting technology has deepened.

Supplementary Information The online version contains supplementary material available at https://doi.org/10.1007/s12520-023-01887-1.

Author contributions W. X. Wang: conceptualization, methodology, formal analysis and investigation, writing—original draft preparation. G. Q. Lu: conceptualization, methodology, formal analysis and investigation, writing—original draft, project administration. S. Jiang: writing—review and editing. P. W. Song: writing—review and editing. Q. Wang: resources, writing—review and editing.

Funding This research is supported by the National Social Science Fund of China (Grant No. 20CKG007), "Youth Interdisciplinary Group Project" of Shandong University (Grant No. 2020QNQT018), The 2022 "Youth Innovation Team Plan" team of higher education institutions in Shandong (China's Early Urban Civilization Research Innovation Team) "Archaeological Discoveries and Urban Civilization Research in ancient capital city site of Zhu state" project (Grant No. 2022RW005) and the Taishan Scholars Program of Shandong (Grant No. 202306023).

Data availability The authors declare that the data supporting the findings of this study are available within the article and its supplementary information files.

Declarations

Competing interests The authors declare no competing interests.

References

Adi EB, Itzhaq S, Lior R, David BS, Shira A, ArenHaskel MMJG (2016) Early Bronze Age pottery covered with lime-plaster: technological observations. J Inst Archaeol Tel Aviv Univ 43:27–42. https://doi.org/10.1080/03344355.2016.1161373

Azizi SN, Yousefpour M (2010) Synthesis of zeolites NaA and analcime using rice husk ash as silica source without using organic template. J Mater Sci 45:5692–5697. https://doi.org/10.1007/s10853-010-4637-7

Cataldo E, Salvi L, Paoli F, Fucile M, Masciandaro G, Manzi D, Masini CM, Mattii GB (2021) Application of zeolites in agriculture and other potential uses: a review. Agronomy 11:1547. https://doi.org/10.3390/agronomy11081547

Chastain ML (2019) The ceramic technology of bronze-casting molds in ancient China: production practices at three Western Zhou foundry sites in the Zhouyuan area. Dissertation, Massachusetts Institute of Technology

Cheng M (2000) The double sided molds of Han Banliang coin found in Zoucheng City, Shandong Province山东邹城市发现汉半两双面范. China Numismatics 中国钱币(02):43. https://doi.org/10.13850/j.cnki.chinum.2000.02.014

Cheng W, Chen S (2022) Bronze casting clay moulds and production sequences: understanding knowledge and organization of the artisans in Late Shang (14th – 11th century BC). China Asian Archaeol 6:137–151. https://doi.org/10.1007/s41826-022-00057-x

Cui Q, Wu G, Kong L, Chen Q, Li X, Lai S, Ding F (2017) Preparation and characterization of hydroxyapatite 羟基磷灰石的制备与表征. J Fujian Normal Univ (Natural Science Edition)福建师范大学学报 (自然科学版) 33:35–39

Cui J (2020) Scientific analysis and research on mirror molds excavated from the Kanjiazhai site in the Linzi city site of Qi state 临淄齐故城阚家寨遗址出土镜范等遗物的科学分析与研究. In: Bai Y, Zheng T (eds) Archaeology of metallurgy and foundry industry in the Linzi city site of Qi state (II) 临淄齐故城冶铸业考古 (中册). Science Press 科学出版社, Beijing, pp 888–907

Dong Y, Ma J, Qin Y, Cen D, Ruan W (2011) Research on the ceramic mold casting techniques of the large-scale iron foundry site at Jia Wan, Xishu 浠水窑家湾大型铸铁遗址的范铸工艺研究. Jianghan Archaeol江汉考古 121(S1):91–106

Flanigen EM, Khatami H, Szymanski HA (1974) Infrared structural studies of zeolite frameworks. In: Edith M, Flanigen, Leonard BS (eds). Molecular sieve zeolites-I. American Chemical Society, Washington, DC, pp 201–229. https://doi.org/10.1021/ba-1971-0101.ch016

Freestone IC, Wood N, Rawson J (1989) Shang Dynasty casting moulds from north China. In: McGovern PE, Notis MD, Kingery WD (eds) Cross craft and cross cultural interactions in ceramics, Ceramics and Civilisation IV. The American Ceramic Society Inc, Westerville, pp 253–275

Ghobarkar H, Schäf O (1999) Effect of temperature on hydrothermal synthesis of analcime and viséite. Mater Sci Eng, B 60:163–167. https://doi.org/10.1016/S0921-5107(99)00012-4

Gooch JW (2011) Dip coating. In: Gooch JW (ed) Encyclopedic dictionary of polymers. Springer, New York. https://doi.org/10.1007/978-1-4419-6247-8_3768

Long B, Li J, Wang Q, Feng S, Zhou G, Feng T, Zhang Y, Xu M, Tian Y, Ma H (2016) CO_2 removal by zeolite molecular sieves 沸石分子筛的CO_2除杂性能. J Tsinghua Univ (Sci Technol) 清华大学学报(自然科学版) 56:824–829. https://doi.org/10.16511/j.cnki.qhdxxb.2016.25.021

Hua J (1982) Discussion on high strength castiron in Han and Wei Dynasties 汉魏高强度铸铁的探讨. Studies in the History of Natural Sciences自然科学史研究 5(1): 1–10

Hua J (1999) Metallurgy in ancient China 中国古代金属技术. Elephant Press 大象出版社, Henan

Huang J (2017) Coin casting techniques in the Eastern Zhou to Han Dynasties evidenced by excavated stone molds 从出土石范看东周至秦汉时期石范铸钱工艺. Journal of National Museum of China中国国家博物馆馆刊 162(01):20–32

Jackson Marie D, Mulcahy Sean R, Chen H, Li Y, Li Q, Cappelletti Piergiulio, Wenk Hans Rudolf (2017) Phillipsite and Al-tobermorite mineral cements produced through low-temperature water-rock reactions in Roman marine concrete. Am Mineral 102:1435–1450. https://doi.org/10.2138/am-2017-5993CCBY

John C (2015) Solidification structure. In: John C (ed) Complete casting handbook, Metal casting processes, metallurgy, techniques and design, 2nd edn. Elsevier, Butterworth-Heinemann, pp 62–222. https://doi.org/10.1016/B978-0-444-63509-9.00005-4

Lever J, Krzywinski M, Altman N (2017) Principal component analysis. Nat Methods 14:641–642. https://doi.org/10.1038/nmeth.4346

Karlbeck O (1935) Anyang moulds. Bullet Museum Far Eastern Antiquities 7:39–60

Kingery WD, Vandiver PB, Prickett M (1988) The beginnings of pyrotechnology, part II: production and use of lime and gypsum plaster in the Pre-Pottery Neolithic Near East. J Field Archaeol 15:219–243. https://doi.org/10.2307/530304

Li J (1991) Excavation report on the Han dynasty iron smelting site at Wafangzhuang, Beiguan, Nanyang南阳北关瓦房庄汉代冶铁遗址发掘报告. Huaxia Archaeol华夏考古 15(01):1–110. https://doi.org/10.16143/j.cnki.1001-9928.1991.01.001

Li Z (2020) Analysis and research on the sand molds excavated from the Kanjiazhai Site in the Linzi city Site of Qi state 临淄齐故城阚家寨遗址出土砂范分析研究. In: Bai Y, Zheng T (eds) Archaeology of metallurgy and foundry industry in the Linzi city site of Qi state (II) 临淄齐故城冶铸业考古 (中册). Science Press 科学出版社, Beijing, pp 985–998

Liu W, Miao C (1995) Natural resources 自然资源. In: Liu W, Miao C (eds) Zoucheng City annals 邹城市志. China Economic Publishing House (中国经济出版社), Beijing, p 91

Liu S, Wang K, Cai Q, Chen J (2013) Microscopic study of Chinese bronze casting moulds from the Eastern Zhou period. J Archaeol Sci 40:2402–2414. https://doi.org/10.1016/j.jas.2012.11.010

Liu Y (2018) Trying to discuss the separate casting technology of bronze ware in Yin ruins 试论殷墟青铜器的分铸技术. Cult Relics Central China中原文物 203:82–89

Liu Y (2019) A technical study of the Yinxu bronze ritual vessels 殷墟出土青铜礼器铸造工艺研究. Guangdong People's Publishing House (广东人民出版社), Guangzhou

Liu Y, Zhang Y, Xu W, Shao A, Chen K (2022) Archaeometallurgical study of iron objects from a third century BC bone workshop in Xianyang, Shaanxi Province. China Archaeol Anthropol Sci 14:71. https://doi.org/10.1007/s12520-022-01538-x

Lu G, Wang Q (2018) The 2015 Excavation of the ancient capital city Site of Zhu state in Zoucheng City, Shandong Province山东邹城市邾国故城遗址2015年发掘简报. Archaeology 考古 606:44–46+126+47–67+2

Lukas N (2006) Imperfect symmetry: re-thinking bronze casting technology in ancient China. Artibus Asiae 66:5–39

Nwaogu UC, Tiedje NS (2011) Foundry coating technology: a review. Mater Sci Appl 2:1143–1160. https://doi.org/10.4236/msa.2011.28155

Routschka G (1997) Lime bricks. In: Routschka G (ed) Pocket manual refractory materials: structure – properties – verification. Vulkan-Verlag, Essen, p 227

Rute S, Ana MR, Kristin G, Alexandre FPF, Alírio ER (2019) Adsorption equilibrium and kinetics of carbon dioxide, methane and nitrogen on binderless zeolite 4A adsorbents. Microporous Mesoporous Mater 277:105–114. https://doi.org/10.1016/j.micromeso.2018.10.024

Tan D, Xu H, Huang L (1999) A study of the techniques of casting with clay molds in bronze age China 中国青铜时代陶范铸造技术研究. Acta Archaeol Sin考古学报 133:211–250

Tankersley KB, Dunning NP, Carr C, Lentz DL, Scarborough VL (2020) Zeolite water purification at Tikal, an ancient Maya city in Guatemala. Sci Rep 10:18021. https://doi.org/10.1038/s41598-020-75023-7

Vikki C, Lior R, Steve W, Elisabetta B (2008) Differentiating between anthropogenic calcite in plaster, ash and natural calcite using infrared spectroscopy: implications in archaeology. J Archaeol Sci 35:905–911. https://doi.org/10.1016/j.jas.2007.06.024

Wang S, Wan Y, Song Z, Yang E, Wang W, Dong C (2012) Forming age of Yishan rock in Luxi area——evidences of SHRIMP zircon dating 鲁西峄山岩体的形成时代——锆石SHRIMP U-Pb定年的证据. Shandong Land Resourc 山东国土资源 28(09):1–6

Wang Q, Wang Y, Liu N, Wu M, Su R, Liu Y (2023) Identification of surface coatings on ceramic bronze-casting moulds from the Houma foundry, Shanxi. China J Archaeol Sci: Reports 48:103858. https://doi.org/10.1016/j.jasrep.2023.103858

Weng S, Xu Y (2016) Fourier transform infrared spectroscopy analysis 傅里叶变换红外光谱分析. Chemical Industry Press化学工业出版社, Beijing, p 412

Yang K (2004) The development of early iron melting furnaces and iron casting technology 早期化铁炉的发展及铸造铁器技术. In: Yang K (ed) The development history of ancient Chinese iron smelting technology (中国古代冶铁技术发展史). Shanghai People's Publishing House上海人民出版社, Shanghai, pp 117–138

Yu H (2021) Construction of bioinspired ordered structured materials by controlled assembly of ultralong hydroxyapatite nanowires and their properties基于羟基磷灰石超长纳米线可控组装构建仿生有序结构材料及其性能研究. Dissertation, University of Chinese Academy of Science(中国科学院大学). https://doi.org/10.27970/d.cnki.gksgs.2021.000010

Yue W, Liu Y, Yue H, Jing Z (2015) Research on the manufacturing technology of Yin ruins ceramic models, moulds, and cores 殷墟陶模、陶范、泥芯的制造工艺研究. Cultural Relics in Southern China 南方文物 95(2):129–140

Zhang M, Hui Q, Lou X, Redfern Simon AT, Salje Ekhard KH, Tarantino Serena C, Seabra Rute, Ribeiro Ana Mafalda, Gleichmann Kristin, Ferreira Alexandre FP, Rodrigues Alírio E (2006) Dehydroxylation, proton migration, and structural changes in heated talc: an infrared spectroscopic study. American Mineralogist 91:816–825. https://doi.org/10.2138/am.2006.1945